nanomaterials

MDPI

Article

Fabrication of Metastable Crystalline Nanocomposites by Flash Annealing of $Cu_{47.5}Zr_{47.5}Al_5$ Metallic Glass Using Joule Heating

Ilya Okulov [1,2,*], Ivan Soldatov [3,4], Ivan Kaban [3], Baran Sarac [5], Florian Spieckermann [6] and Jürgen Eckert [5,6]

1 Faculty of Production Engineering, University of Bremen, Badgasteiner Street 1, 2, 28359 Bremen, Germany
2 Leibniz Institute for Materials Engineering—IWT, Badgasteiner Street 3, 28359 Bremen, Germany
3 Leibniz Institute for Solid State and Materials Research IFW Dresden, Helmholtzstrasse 20, 01069 Dresden, Germany; i.soldatov@ifw-dresden.de (I.S.); i.kaban@ifw-dresden.de (I.K.)
4 Institute of Natural Sciences and Mathematics, Ural Federal University, 620002 Yekaterinburg, Russia
5 Erich Schmid Institute of Materials Science, Austrian Academy of Sciences, Jahnstraße 12, 8700 Leoben, Austria; baran.sarac@oeaw.ac.at (B.S.); juergen.eckert@unileoben.ac.at (J.E.)
6 Department of Materials Science, University of Leoben, Jahnstraße 12, 8700 Leoben, Austria; florian.spieckermann@unileoben.ac.at
* Correspondence: i.okulov@iwt.uni-bremen.de or okulovilya@yandex.ru

Received: 26 November 2019; Accepted: 26 December 2019; Published: 1 January 2020

Abstract: Flash Joule-heating was applied to the $Cu_{47.5}Zr_{47.5}Al_5$ metallic glass for designing fully crystalline metastable nanocomposites consisting of the metastable B2 CuZr and low-temperature equilibrium $Cu_{10}Zr_7$ phases. The onset of crystallization was in situ controlled by monitoring resistivity changes in the samples. The effect of heating rate and annealing time on the volume fraction of the crystalline phases and mechanical properties of the nanocomposites was studied in detail. Particularly, an increase of the heating rate and a decrease of the annealing time lead to a lower number of equilibrium $Cu_{10}Zr_7$ precipitates and an increase of tensile ductility. Tailoring of these non-equilibrium microstructures and mechanical properties may not be possible unless one starts with a fully glassy material that opens new perspectives for designing metastable nanomaterials with unique physical properties.

Keywords: nanocomposite; metallic glass; flash annealing; metastable material; mechanical behaviour

1. Introduction

For several decades, composite materials [1–6] and materials with composite microstructures [7–9] have been the focus of research and industry as they provide a whole range of complementary physical properties determined by matrix and non-matrix counterparts. In many cases, the properties of composite materials even exceed the properties of their constituent materials. Some examples include anomalously low elastic modulus in Fe-Mg microcomposites [10], outstanding strength in metal-polymer nanocomposites [5,11–13] fabricated from nanoporous metals [14–19], and significantly enhanced plastic deformability in metallic glass composites [20,21]. The design of non-equilibrium composite microstructures in as-cast nanostructured titanium alloys [22–26] leads to the high strength and good plastic deformability required for structural and biomedical applications [27,28]. One of the promising processing methods for the design of advanced materials with non-equilibrium composite microstructures is the annealing of metallic glasses [21,29].

Metallic glasses are metallic solids with disordered, liquid-like atomic structures. Thermodynamically, metallic glasses are in a high-energy (metastable) state regardless of their

fabrication method and, consequently, they can be easily transformed into more stable crystalline states by lowering their energy. Among the exciting applications making use of annealing of metallic glasses is the development of nanostructured FINEMET material [8] with superior magnetic properties. Some further examples of composite-structured materials based on metallic glasses can be found in [30–32]. It is important to note that, usually, phase transformations in metallic glasses occur rapidly and, thus, rapid annealing methods have to be used in order to control these transformations.

Recently, flash-annealing techniques based on Joule [20], inductive [33,34], and electromagnetic radiation [35] heating were reported as tools for controllable tuning of the microstructure in metallic glass ribbons and bulk samples, respectively, aiming to improve their mechanical properties. Both techniques were applied to CuZr-based metallic glasses, which were partially devitrified into the metastable B2 CuZr structure to form glass-matrix composites. The thus obtained homogeneously distributed B2 CuZr crystals in the glassy matrix result in a significant improvement of the mechanical properties of the CuZr-based metallic glasses and even allow for tailoring the tensile ductility [20]. Furthermore, it has been shown that the strength of fully crystalline composites containing ultrafine-grained crystalline phases even exceeds that of the parent glass [20].

In this study, we focus on the effect of heating rate and time on the formation of stable and metastable crystalline phases in the $Cu_{47.5}Zr_{47.5}Al_5$ metallic glass upon flash annealing and the mechanical properties of the crystalline nano- and microcomposites obtained.

2. Materials and Methods

Samples were prepared under high purity argon atmosphere in two steps. First, $Cu_{47.5}Zr_{47.5}Al_5$ (at. %) ingots were produced from Cu (99.99%), Zr (99.98%), and Al (99.99%), by arc-melting. In the second step, glassy ribbons were prepared from the ingots by melt-spinning. The metallic glass ribbons were annealed using an in-house designed set-up. The samples were characterized by X-ray diffraction (XRD, Stoe, STADI P with Mo-Kα1 radiation, Darmstadt, Germany) and scanning electron microscopy (SEM, Zeiss, Leo Gemini 1530, Oberkochen, Germany). Phase identification was done by means of the X'Pert High Score Plus (Malvern Panalytical, Malvern, UK) software, whereas SEM images were analysed using ImageJ (open source) software. Mechanical testing was performed with an Instron 8562 machine (Instron, Norwood, MA, United States) at a strain rate of 10^{-4} s^{-1} at room temperature. The strain was measured by a laser extensometer (Fiedler Optoelektronik, Lützen, Germany). The gauge length of 5 mm was selected in the middle region of a ribbon sample.

3. Results and Discussion

$Cu_{47.5}Zr_{47.5}Al_5$ metallic glass can transform to a lower energy state through several devitrification paths. These are schematically illustrated in a continuous heating transformation (CHT) diagram in Figure 1.

Fast heating to temperatures above the crystallization temperature, T_x, as depicted by line 1, leads to nucleation of the metastable B2 CuZr phase in the metallic glass matrix. Fast cooling is required to avoid decomposition of B2 CuZr into the thermodynamically favourable low temperature eutectic phases (LT-EPs) $Cu_{10}Zr_7$ and $CuZr_2$, and thus to stabilize B2 CuZr at room temperature. The ductile B2 CuZr crystals hinder localization of deformation in the glassy phase leading to tensile ductility of the glass-matrix composites [20]. Moving the cooling curve closer to the nose of the stability regime of the LT-EPs leads to a higher solid fraction of B2 CuZr, ultimately leading to complete suppression of the glassy phase. Heating along line 2 and cooling along lines a and b results in devitrification of the metallic glass into B2 CuZr with subsequent decomposition of B2 CuZr into the LT-EPs. As it has been shown in earlier works [20,33], the mechanical properties of the composites obtained depend strongly on the constituent phases.

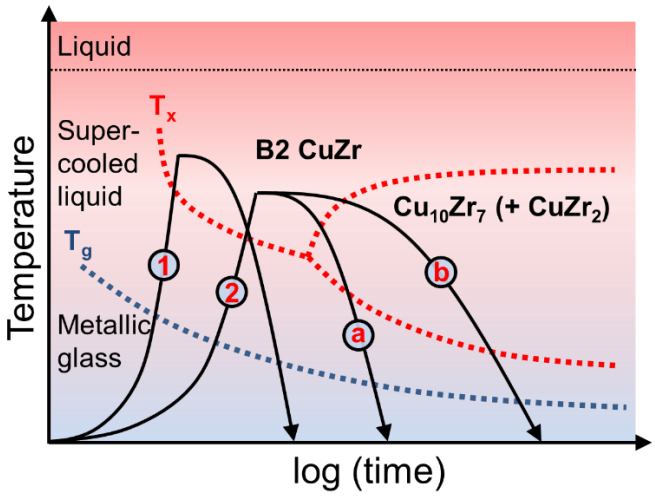

Figure 1. Schematic continuous heating transformation (CHT) diagram of the $Cu_{47.5}Zr_{47.5}Al_5$ metallic glass based on [20].

In this work, we use the Joule heating for annealing of the $Cu_{47.5}Zr_{47.5}Al_5$ metallic glass. Hereby, an electrical current is applied to a sample for a short time from several milliseconds to a few seconds, as described elsewhere [20]. The fast heating is favoured by the rather high resistivity of metallic glasses [36,37]. Since crystalline phases possess a higher conductivity compared to their glassy counterparts, devitrification of the glassy phase leads to a remarkable resistivity drop, which allows one to quite sensitively monitor crystallization processes [20]. The distribution of the applied current density versus the onset of the resistivity drop for the $Cu_{47.5}Zr_{47.5}Al_5$ metallic glass can be found in our previous study [20]. The relatively short heating time during the Joule heating allows the adiabatic conditions to be nearly fulfilled and, therefore, the current density is proportional to the heating rate, as has been proven by measurement of heating rates using a thermocouple. The heating rates given in Table 1 have been estimated based on the crystallization temperature of the $Cu_{47.5}Zr_{47.5}Al_5$ metallic glass (about 695 K at about 0.7 K s^{-1} heating rate) [38], and the measured time-to-crystallisation indicated by the resistivity drop. Particularly, the heating rate corresponding to the highest applied current density (namely, 59 ± 5 MA m^{-2}) is ≥830 K s^{-1}.

Table 1. Microstructural characteristics of the $Cu_{47.5}Zr_{47.5}Al_5$ metallic glass samples rapidly annealed until the resistivity drop.

Sample	Current Density (MA m^{-2})	Estimated Heating Rate (K s^{-1})	Annealing Time	Volume Fraction of B2 CuZr (vol.%)	Volume Fraction of $Cu_{10}Zr_7$ (vol.%)	Number of $Cu_{10}Zr_7$ Particles (mm^{-2})	Size of $Cu_{10}Zr_7$ Particles (μm)
B2-98	59 ± 5	≥830	Until resistivity drop	98 ± 1	2 ± 1	1.1×10^4 ± 0.1	2.3 ± 0.3
B2-83	44 ± 5	≥330		83 ± 3	17 ± 3	22.0×10^4 ± 0.7	1.7 ± 0.2
B2-59	34 ± 5	≥150		59 ± 5	41 ± 5	61.2×10^4 ± 1.5	1.1 ± 0.3
B2-27	34 ± 5	≥150	1.6 s after resistivity drop	27 ± 4	73 ± 4	146.9×10^4 ± 2.8	1.2 ± 0.2
B2-11	34 ± 5	≥150	2.2 s after resistivity drop	11 ± 3	89 ± 3	169.5×10^4 ± 2.1	1.0 ± 0.2

Figure 2 displays the effect of the heating rate (current density) on the microstructure of the flash-annealed $Cu_{47.5}Zr_{47.5}Al_5$ metallic glass. X-ray diffraction analysis of the samples annealed at the lowest heating rate (≥150 K s^{-1}) reveals the presence of two crystalline phases: the low-temperature equilibrium $Cu_{10}Zr_7$ and the metastable B2 CuZr phases (Figure 2a). As the heating rate increases above 330 K s^{-1}, the intensity of $Cu_{10}Zr_7$ reflections decreases significantly, indicating a lower content of this phase in the sample (Figure 2b). Finally, at a heating rate of ≥830 K s^{-1}, there are no detectable peaks of the $Cu_{10}Zr_7$ phase and the sample mainly consists of the metastable B2 CuZr phase (Figure 2c).

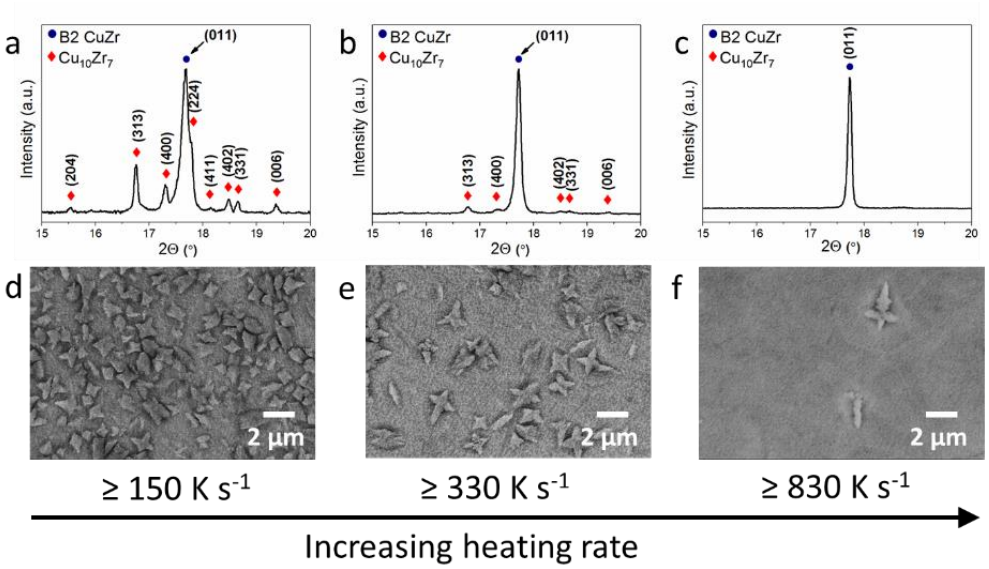

Figure 2. Effect of heating rate on the microstructure of flash annealed $Cu_{47.5}Zr_{47.5}Al_5$ metallic glass. XRD patterns (**a**–**c**) and secondary electron SEM micrographs (**d**–**f**) of the $Cu_{47.5}Zr_{47.5}Al_5$ metallic glass samples rapidly annealed by Joule heating (up to the resistivity drop) with the following current densities: (**a**,**d**) 34 ± 5 MA m^{-2}; (**b**,**e**) 44 ± 5 MA m^{-2}; and (**c**,**f**) and 59 ± 5 MA m^{-2}. (Figure 2d is adopted from [20]).

Figure 2d–f demonstrates the microstructure of the annealed $Cu_{47.5}Zr_{47.5}Al_5$ metallic glass samples. The samples consist of dendritic $Cu_{10}Zr_7$ crystals that are homogeneously distributed in a B2 CuZr matrix. The volume fraction of the $Cu_{10}Zr_7$ dendrites increases with decreasing heating rate from about 2 ± 1 vol.% (≥830 K s^{-1}) to 17 ± 3 vol.% (≥330 K s^{-1}), finally reaching 41 ± 5 vol.% at the lowest heating rate (≥150 K s^{-1}) (Table 1). The size of the $Cu_{10}Zr_7$ dendrites also depends on the applied heating rate or current density. A larger dendrite size is achieved at a higher heating rate and vice versa. For example, the mean dendrite size in the sample subjected to the highest heating rate ≥830 K s^{-1} is 2.3 ± 0.2 μm, while it drops to 1.1 ± 0.3 μm for the samples obtained at the heating rate ≥150 K s^{-1} (Table 1). Along with the volume fraction and size of the $Cu_{10}Zr_7$ crystals, their number increases with higher heating rate from about 1.1×10^4 to 22.0×10^4 and reaches 61.2×10^4 particles per mm^2.

The volume fraction of $Cu_{10}Zr_7$ dendrites in the B2 CuZr matrix can also be tuned by controlling the annealing time at a constant current density (heating rate), as shown in Figure 3. To reveal this effect, several samples annealed (i) until the resistivity drop, (ii) 1.6 s after the resistivity drop, and (iii) 2.2 s after the resistivity drop at a current density i_3 = 34 ± 5 MA m^{-2} (≥150 K s^{-1}) were selected. X-ray analysis indicates the presence of two phases in these samples, namely, the low-temperature equilibrium $Cu_{10}Zr_7$ phase and the metastable B2 CuZr phase. The intensity of the B2 CuZr phase peaks is highest for the samples annealed until the resistivity drop. A relatively small increase in annealing time (1.6–2.2 s) leads to a higher intensity of the $Cu_{10}Zr_7$ peaks. This is in agreement with the findings from secondary electron micrographs (Figure 3d–e). The increase of annealing time at the constant heating rate (≥150 K s^{-1}) leads to a higher volume fraction and a larger number of $Cu_{10}Zr_7$ dendrites (Table 1). Particularly, the volume fraction of the $Cu_{10}Zr_7$ dendrites increases from 41 ± 5 to

89 ± 3 vol.% for the annealing times until the resistivity drop and 2.2 s after the drop, respectively. In contrast to the effect of heating rate, the size of the $Cu_{10}Zr_7$ dendrites varies insignificantly for different annealing times. These findings suggest that the volume fraction, number, and size of the $Cu_{10}Zr_7$ crystals strongly depend on the specific heat treatment conditions and can be tuned by varying the current density being proportional to the heating rate.

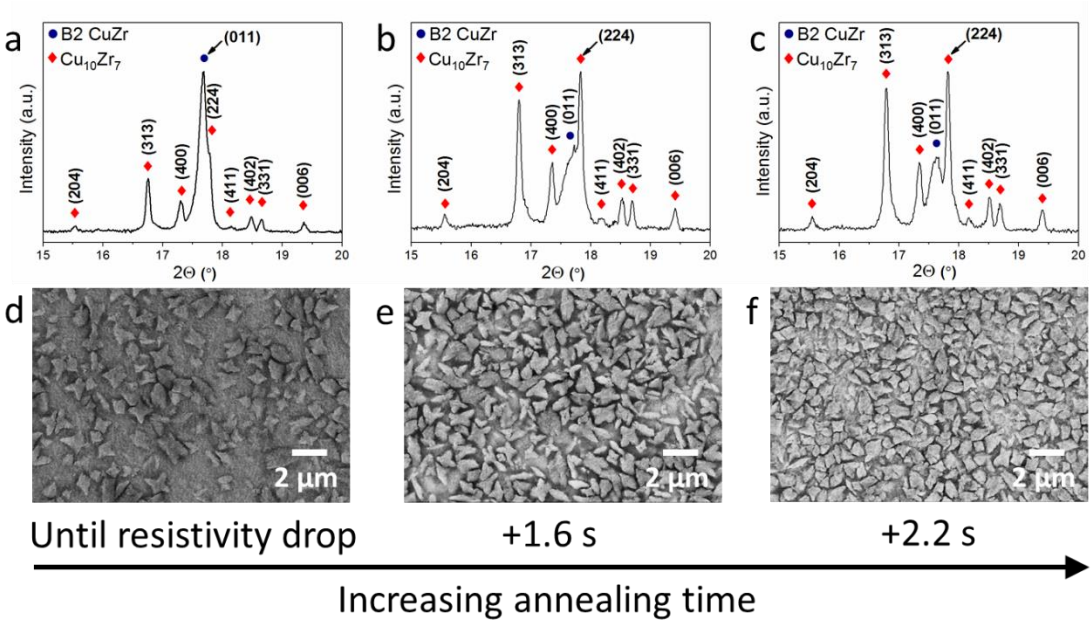

Figure 3. Effect of annealing time on the microstructure of flash annealed $Cu_{47.5}Zr_{47.5}Al_5$ metallic glass. X-ray diffractograms (**a**–**c**) and secondary electron micrographs (**d**–**f**) of the $Cu_{47.5}Zr_{47.5}Al_5$ metallic glass samples rapidly annealed by Joule heating at the current density $i_3 = 34 \pm 5$ MA m^{-2} and different times: (**a**,**d**) until the resistivity drop; (**b**,**e**) 1.6 s after the resistivity drop; and (**c**,**f**) 2.2 s after the resistivity drop. (Figure 3d is adopted from [20]).

In the current study, the flash Joule heating of the $Cu_{47.5}Zr_{47.5}Al_5$ metallic glass leads to its devitrification into two phases: metastable B2 CuZr and equilibrium $Cu_{10}Zr_7$. This finding is in contrast to the equilibrium phase diagram [39] and some experimental as well as theoretical studies on the devitrification sequence of CuZr-based metallic glasses [33,35,38,40]. Based on theoretical considerations, Kaban et al. suggested that the $Cu_{47.5}Zr_{47.5}Al_5$ metallic glass devitrifies following the sequence $Cu_{10}Zr_7 \rightarrow CuZr_2 \rightarrow$B2 CuZr [40]. Experimental studies show that the $Cu_{47.5}Zr_{47.5}Al_5$ metallic glass directly transforms into the $Cu_{10}Zr_7$ and $CuZr_2$ equilibrium phases upon annealing at low heating rates of 10–40 K min^{-1}, while the $CuZr_2$ phase precipitates after the $Cu_{10}Zr_7$ phase [38]. Recent reports demonstrated that rapid annealing of the $Cu_{47.5}Zr_{47.5}Al_5$ metallic glass can suppress the formation of the low-temperature equilibrium phases completely [33] or partially [20], leading to its transformation into the non-equilibrium B2 CuZr phase. In the latter case, the $Cu_{10}Zr_7$ crystals are found within the B2 CuZr precipitates but the second equilibrium $CuZr_2$ phase is not observed. According to the devitrification experiments and theoretical studies [38,40], the $CuZr_2$ phase precipitates after $Cu_{10}Zr_7$, and, therefore, it can be assumed that in the current flash annealing case, the conditions for the precipitation of the $CuZr_2$ phase are not fulfilled. The $CuZr_2$ phase requires a specific stoichiometry for nucleation, which is probably not achieved during the short processing time.

The annealing conditions such as annealing temperature and time affect the nucleation and growth rate of precipitates. The growth rate is determined by the rate of diffusion and, therefore, it increases with increasing temperature [41]. The nucleation rate is also temperature-dependent and exhibits a maximum in an intermediate temperature range (Figure 4). According to the obtained results, the number of $Cu_{10}Zr_7$ dendrites decreases while their average size increases at higher heating rate. This

suggests that the B2-98 sample with the lowest number ($1.1 \times 10^4 \pm 0.1 \times mm^{-2}$) and the largest size ($2.3 \pm 0.3$ µm) of $Cu_{10}Zr_7$ dendrites was subjected to the highest transformation temperature. A decrease of the heating rate leads to a larger number of $Cu_{10}Zr_7$ dendrites, which also become finer. This can be explained by a decrease of the average transformation temperature, which seems to be dependent on heating rate. The lowest applied heating rate (here, 150 K s^{-1}) corresponds to the most optimum average transformation temperature for the highest nucleation rate. Therefore, increasing the annealing time in this case leads to a significant increase of the number of $Cu_{10}Zr_7$ dendrites.

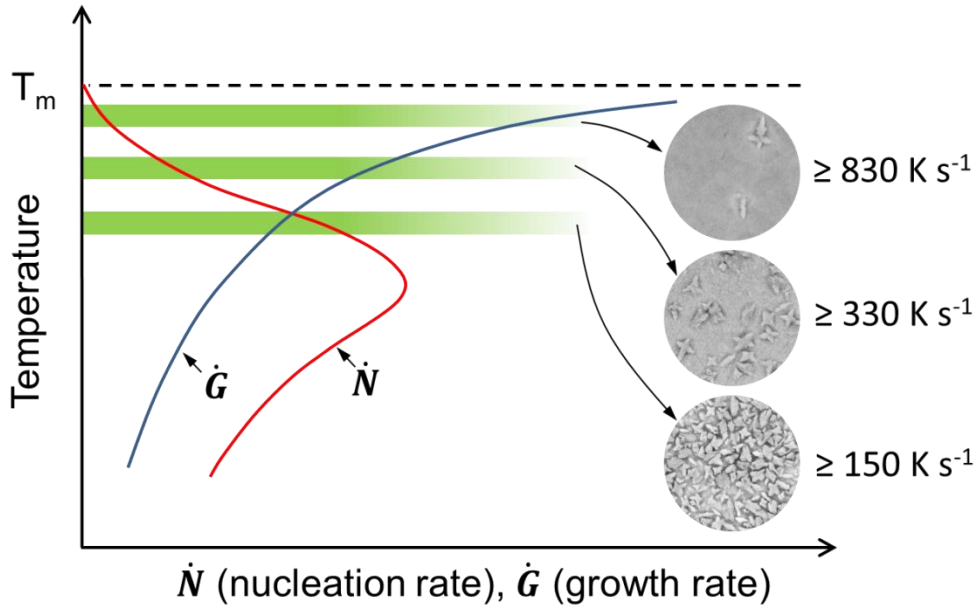

Figure 4. Schematic illustration of annealing conditions of the samples selected for the current study. Nucleation and growth rate curves are drawn based on reference [41].

Tailored by flash annealing of the $Cu_{47.5}Zr_{47.5}Al_5$ metallic glass, the composite microstructure of the current samples leads to notable tensile deformability and high strength (Figure 5) comparable with that of metallic glass matrix composites [20,33]. Moreover, the crystalline samples exhibit pronounced strain-hardening behaviour. The yield strength of the samples increases from 700 ± 30 to 1440 ± 30 MPa with increasing volume fraction of $Cu_{10}Zr_7$ dendrites (Table 2). This strength increase with increasing volume fraction of $Cu_{10}Zr_7$ dendrites is at the cost of tensile deformability: the strain-to-fracture decreases form 7.1 ± 0.5 to 1.8 ± 0.2% when the volume fraction of $Cu_{10}Zr_7$ dendrites increases from 2 ± 1 to 73 ± 4 vol.%. However, these fracture strain values are still in the range of interest for technological applications. For example, the B2-83 sample exhibits a tensile ductility of 7.5 ± 0.5%. Due to increasing strain hardening, the ultimate tensile strength increases from 1580 ± 50 to 1710 ± 50 MPa with higher volume fraction and number of $Cu_{10}Zr_7$ dendrites in the B2 CuZr matrix (Table 2).

Table 2. Mechanical properties of the $Cu_{10}Zr_7$ dendrite/B2 nano- and microcomposites obtained by flash annealing the $Cu_{47.5}Zr_{47.5}Al_5$ metallic glass.

Sample	Yield Strength (MPa)	Ultimate Tensile Strength (MPa)	Young's Modulus (GPa)	Strain to Fracture (%)
B2-27	1440 ± 30	1580 ± 50	94.9 ± 0.6	1.8 ± 0.2
B2-59	1220 ± 30	1670 ± 50	94.3 ± 0.4	2.7 ± 0.1
B2-83	980 ± 30	1710 ± 50	87.2 ± 0.4	7.5 ± 0.5
B2-98	700 ± 30	1320 ± 50	79.5 ± 0.8	7.1 ± 0.5

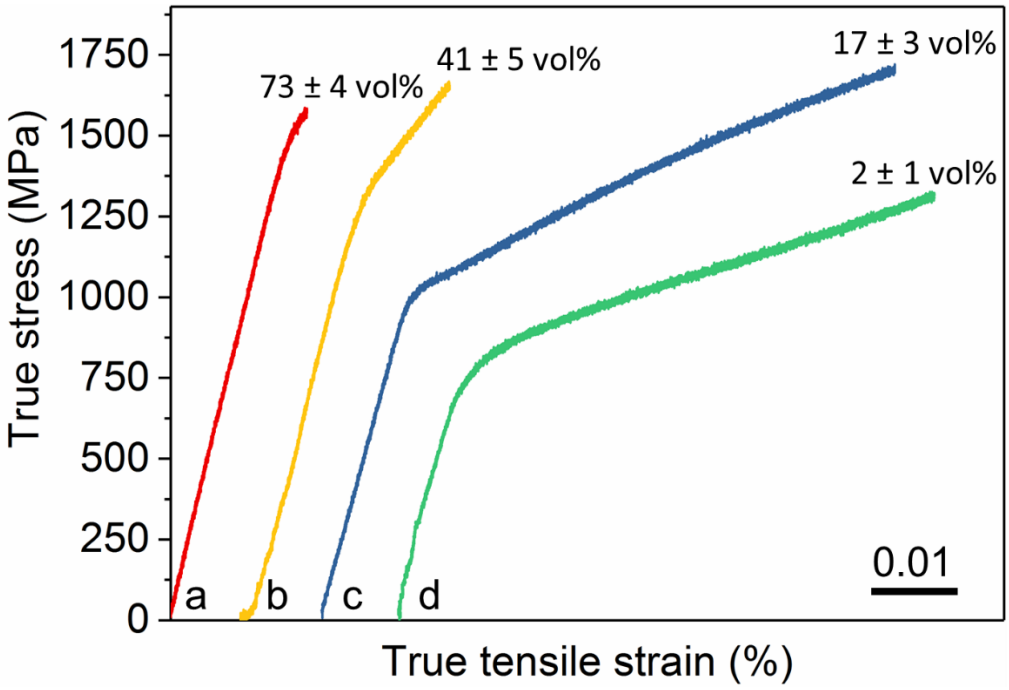

Figure 5. Room temperature tensile true stress-true strain curves of the $Cu_{10}Zr_7$ dendrite/B2 nano- and microcomposites obtained by flash annealing the $Cu_{47.5}Zr_{47.5}Al_5$ metallic glass. (a) Annealed at 34 ± 5 MA m^{-2} until 1.6 s after the onset of the resistivity drop; (b) annealed at 34 ± 5 MA m^{-2} until the resistivity drop; (c) annealed at 44 ± 5 MA m^{-2} until the resistivity drop; and (d) annealed at 59 ± 5 MA m^{-2} until resistivity drop. The values at the end of the stress-strain curves indicate the volume fraction of the $Cu_{10}Zr_7$ dendrites. (Stress-strain curve "d" is adopted from [20]).

4. Conclusions

In summary, we have tailored different microstructures by devitrification of the $Cu_{47.5}Zr_{47.5}Al_5$ metallic glass using flash Joule annealing. The size and volume fraction of the constituent phases—metastable B2 CuZr and equilibrium $Cu_{10}Zr_7$—can be flexibly tuned by optimizing the heating rate and annealing time. The strength of the $Cu_{10}Zr_7$/B2 nanocomposites obtained through flash Joule heating and annealing exceeds that of the initial metallic glass and is comparable with that of metallic glass matrix composites. Hence, glassy materials provide a unique base for obtaining non-equilibrium microstructures by flash annealing with technologically attractive properties that cannot be achieved through conventional processing.

Author Contributions: Conceptualization, I.O., I.S., J.E., and I.K.; methodology, I.O. and I.S.; software, I.S.; formal analysis, I.O. and I.S.; investigation, I.O. and I.S.; writing—original draft preparation, I.O.; writing—review and editing, I.O., I.S., J.E., I.K., F.S., and B.S.; supervision, J.E.; funding acquisition, J.E. All authors have read and agreed to the published version of the manuscript.

Funding: This research was funded by the German Federal Ministry of Education and Science BMBF, grant number 05K2012, the German Science Foundation under the Leibniz Program, grant numbers EC 111/26-1 and MA 3333/13-1, and the European Research Council (ERC) under the ERC Advanced Grant INTELHYB, grant number ERC-2013-ADG-340025.

Acknowledgments: The authors are grateful to S. Donath, F. Ebert, M. Frey, and B. Opitz for technical assistance and kindly acknowledge O. Shuleshova, N. Mattern, and L.B. Bruno for valuable discussions.

Conflicts of Interest: The authors declare no conflict of interest.

References

1. Miracle, D.B.; Donaldson, S.L. ASM Handbook: Composite. In *ASM Handbook*; ASM International: Material Park, OH, USA, 2001; ISBN 9780871707031.

2. Skrotzki, W.; Eschke, A.; Romberg, J.; Scharnweber, J.; Marr, T.; Petters, R.; Okulov, I.; Oertel, C.-G.; Freudenberger, J.; Kühn, U.; et al. Processing of High Strength Light-Weight Metallic Composites. *Adv. Eng. Mater.* **2014**, *16*, 1208–1216. [CrossRef]
3. Okulov, I.V.; Weissmüller, J.; Markmann, J. Dealloying-based interpenetrating-phase nanocomposites matching the elastic behavior of human bone. *Sci. Rep.* **2017**, *7*, 20. [CrossRef]
4. Marr, T.; Freudenberger, J.; Seifert, D.; Klauß, H.; Romberg, J.; Okulov, I.; Scharnweber, J.; Eschke, A.; Oertel, C.-G.; Skrotzki, W.; et al. Ti-Al Composite Wires with High Specific Strength. *Metals* **2011**, *1*, 79–97. [CrossRef]
5. Wang, K.; Kobler, A.; Kübel, C.; Jelitto, H.; Schneider, G.; Weissmüller, J. Nanoporous-gold-based composites: Toward tensile ductility. *NPG Asia Mater.* **2015**, *7*, 187. [CrossRef]
6. Marr, T.; Freudenberger, J.; Kauffmann, A.; Romberg, J.; Okulov, I.; Petters, R.; Scharnweber, J.; Eschke, A.; Oertel, C.-G.; Kühn, U.; et al. Processing of intermetallic titanium aluminide wires. *Metals* **2013**, *3*, 188–201. [CrossRef]
7. Okulov, I.V.; Bönisch, M.; Volegov, A.S.; Shahabi Shakur, H.; Wendrock, H.; Gemming, T.; Eckert, J. Micro-to-nano-scale deformation mechanism of a Ti-based dendritic-ultrafine eutectic alloy exhibiting large tensile ductility. *Mater. Sci. Eng. A* **2017**, *682*, 673–678. [CrossRef]
8. Yoshizawa, Y.; Oguma, S.; Yamauchi, K. New Fe-based soft magnetic alloys composed of ultrafine grain structure. *J. Appl. Phys.* **1988**, *64*, 6044. [CrossRef]
9. Hofmann, D.C.; Suh, J.-Y.; Wiest, A.; Duan, G.; Lind, M.-L.; Demetriou, M.D.; Johnson, W.L. Designing metallic glass matrix composites with high toughness and tensile ductility. *Nature* **2008**, *451*, 1085–1089. [CrossRef] [PubMed]
10. Okulov, I.V.; Geslin, P.-A.; Soldatov, I.V.; Ovri, H.; Joo, S.-H.; Kato, H. Anomalously low modulus of the interpenetrating-phase composite of Fe and Mg obtained by liquid metal dealloying. *Scr. Mater.* **2019**, *163*, 133–136. [CrossRef]
11. Okulov, A.V.; Volegov, A.S.; Weissmüller, J.; Markmann, J.; Okulov, I.V. Dealloying-based metal-polymer composites for biomedical applications. *Scr. Mater.* **2018**, *146*, 290–294. [CrossRef]
12. Okulov, I.V.; Okulov, A.V.; Volegov, A.S.; Markmann, J. Tuning microstructure and mechanical properties of open porous TiNb and TiFe alloys by optimization of dealloying parameters. *Scr. Mater.* **2018**, *154*, 68–72. [CrossRef]
13. Wang, K.; Weissmüller, J. Composites of nanoporous gold and polymer. *Adv. Mater.* **2013**, *25*, 1280–1284. [CrossRef] [PubMed]
14. Wada, T.; Yubuta, K.; Inoue, A.; Kato, H. Dealloying by metallic melt. *Mater. Lett.* **2011**, *65*, 1076–1078. [CrossRef]
15. Okulov, I.V.; Lamaka, S.V.; Wada, T.; Yubuta, K.; Zheludkevich, M.L.; Weissmüller, J.; Markmann, J.; Kato, H. Nanoporous magnesium. *Nano Res.* **2018**, *11*, 6428–6435. [CrossRef]
16. Joo, S.-H.; Bae, J.W.; Park, W.-Y.; Shimada, Y.; Wada, T.; Kim, H.S.; Takeuchi, A.; Konno, T.J.; Kato, H.; Okulov, I.V. Beating Thermal Coarsening in Nanoporous Materials via High-Entropy Design. *Adv. Mater.* **2019**. [CrossRef]
17. Okulov, I.V.; Okulov, A.V.; Soldatov, I.V.; Luthringer, B.; Willumeit-Römer, R.; Wada, T.; Kato, H.; Weissmüller, J.; Markmann, J. Open porous dealloying-based biomaterials as a novel biomaterial platform. *Mater. Sci. Eng. C* **2018**, *83*, 95–103. [CrossRef]
18. Shi, S.; Markmann, J.; Weissmüller, J. Actuation by hydrogen electrosorption in hierarchical nanoporous palladium. *Philos. Mag.* **2017**, *97*, 1571–1587. [CrossRef]
19. Lührs, L.; Soyarslan, C.; Markmann, J.; Bargmann, S.; Weissmüller, J. Elastic and plastic Poisson's ratios of nanoporous gold. *Scr. Mater.* **2016**, *110*, 65–69. [CrossRef]
20. Okulov, I.V.; Soldatov, I.V.; Sarmanova, M.F.; Kaban, I.; Gemming, T.; Edström, K.; Eckert, J. Flash Joule heating for ductilization of metallic glasses. *Nat. Commun.* **2015**, *6*, 7932. [CrossRef]
21. Louzguine-Luzgin, D.V.; Inoue, A. Nano-Devitrification of Glassy Alloys. *J. Nanosci. Nanotechnol.* **2005**, *5*, 999–1014. [CrossRef]

22. Okulov, I.V.; Sarmanova, M.F.; Volegov, A.S.; Okulov, A.; Kühn, U.; Skrotzki, W.; Eckert, J. Effect of boron on microstructure and mechanical properties of multicomponent titanium alloys. *Mater. Lett.* **2015**, *158*, 111–114. [CrossRef]
23. Okulov, I.V.; Kühn, U.; Marr, T.; Freudenberger, J.; Soldatov, I.V.; Schultz, L.; Oertel, C.-G.; Skrotzki, W.; Eckert, J. Microstructure and mechanical properties of new composite structured Ti–V–Al–Cu–Ni alloys for spring applications. *Mater. Sci. Eng. A* **2014**, *603*, 76–83. [CrossRef]
24. Okulov, I.V.; Kühn, U.; Romberg, J.; Soldatov, I.V.; Freudenberger, J.; Schultz, L.; Eschke, A.; Oertel, C.-G.; Skrotzki, W.; Eckert, J. Mechanical behavior and tensile/compressive strength asymmetry of ultrafine structured Ti–Nb–Ni–Co–Al alloys with bi-modal grain size distribution. *Mater. Des.* **2014**, *62*, 14–20. [CrossRef]
25. Okulov, I.V.; Bönisch, M.; Okulov, A.V.; Volegov, A.S.; Attar, H.; Ehtemam-Haghighi, S.; Calin, M.; Wang, Z.; Hohenwarter, A.; Kaban, I.; et al. Phase formation, microstructure and deformation behavior of heavily alloyed TiNb- and TiV-based titanium alloys. *Mater. Sci. Eng. A* **2018**, *733*, 80–86. [CrossRef]
26. Louzguine, D.V.; Kato, H.; Inoue, A. High strength and ductile bulk Ti–Ni–Cu–Nb alloy with submicron-size structure units obtained by arc-melting. *J. Alloy. Compd.* **2004**, *375*, 171–174. [CrossRef]
27. Okulov, I.V.; Volegov, A.S.; Attar, H.; Bönisch, M.; Calin, M.; Eckert, J. Composition optimization of low modulus and high-strength TiNb-based alloys for biomedical applications. *J. Mech. Behav. Biomed. Mater.* **2017**, *65*, 866–871. [CrossRef] [PubMed]
28. Okulov, I.V.; Pauly, S.; Kühn, U.; Gargarella, P.; Marr, T.; Freudenberger, J.; Schultz, L.; Scharnweber, J.; Oertel, C.-G.; Skrotzki, W.; et al. Effect of microstructure on the mechanical properties of as-cast Ti–Nb–Al–Cu–Ni alloys for biomedical application. *Mater. Sci. Eng. C* **2013**, *33*, 4795–4801. [CrossRef]
29. Orava, J.; Kaban, I.; Benkocka, M.; Han, X.; Soldatov, I.; Greer, A.L. Fast-heating-induced formation of metallic-glass/crystal composites with enhanced plasticity. *Thermochim. Acta* **2019**, *677*, 198–205. [CrossRef]
30. Allia, P.; Baricco, M.; Knobel, M.; Vinai, F. Soft nanocrystalline ferromagnetic alloys with improved ductility obtained through dc Joule heating of amorphous ribbons. *J. Magn. Magn. Mater.* **1994**, *133*, 243–247. [CrossRef]
31. Allia, P.; Tiberto, P.; Baricco, M.; Vinai, F. dc Joule heating of amorphous metallic ribbons: Experimental aspects and model. *Rev. Sci. Instrum.* **1993**, *64*, 1053. [CrossRef]
32. Allia, P.; Tiberto, P.; Baricco, M.; Vinai, F. Improved ductility of nanocrystalline Fe73.5Nb3Cu1Si13.5B9 obtained by direct-current joule heating. *Appl. Phys. Lett.* **1993**, *63*, 2759. [CrossRef]
33. Kosiba, K.; Scudino, S.; Kobold, R.; Kühn, U.; Greer, A.L.; Eckert, J.; Pauly, S. Transient nucleation and microstructural design in flash-annealed bulk metallic glasses. *Acta Mater.* **2017**, *127*, 416–425. [CrossRef]
34. Kosiba, K.; Pauly, S. Inductive flash-annealing of bulk metallic glasses. *Sci. Rep.* **2017**, *7*, 2151. [CrossRef] [PubMed]
35. Song, K.K.; Han, X.L.; Pauly, S.; Qin, Y.S.; Kosiba, K.; Peng, C.X.; Gong, J.H.; Chen, P.X.; Wang, L.; Sarac, B.; et al. Rapid and partial crystallization to design ductile CuZr-based bulk metallic glass composites. *Mater. Des.* **2018**, *139*, 132–140. [CrossRef]
36. Smili, B.; Messaoud, A.; Bouchelaghem, W.; Abadlia, L.; Fazel, N.; Benmoussa, A.; Kaban, I.; Gasser, F.; Gasser, J.G. Temperature dependence of the electrical resistivity and absolute thermoelectric power of amorphous metallic glass Ni33.3Zr66.7. *J. Non. Cryst. Solids* **2018**, *481*, 352–360. [CrossRef]
37. Kaban, I.; Khalouk, K.; Gasser, F.; Gasser, J.-G.; Bednarčik, J.; Shuleshova, O.; Okulov, I.; Gemming, T.; Mattern, N.; Eckert, J. In situ studies of temperature-dependent behaviour and crystallisation of Ni36.5Pd36.5P27 metallic glass. *J. Alloy. Compd.* **2014**, *615*, S208–S212. [CrossRef]
38. Pauly, S.; Das, J.; Mattern, N.; Kim, D.H.; Eckert, J. Phase formation and thermal stability in Cu–Zr–Ti(Al) metallic glasses. *Intermetallics* **2009**, *17*, 453–462. [CrossRef]
39. Tretyachenko, L. Al-Cu-Zr (Aluminium-Copper-Zirconium). In *Light Metal Ternary Systems: Phase Diagrams, Crystallographic and Thermodynamic Data*; Effenberg, G., Ilyenko, S., Eds.; Landolt-Börnstein—Group IV Physical Chemistry; SpringerMaterials—The Landolt-Börnstein Database; Springer: Berlin/Heidelberg, Germany, 2014; Volume 11A2, pp. 206–223.

40. Kaban, I.; Jóvári, P.; Escher, B.; Tran, D.T.; Svensson, G.; Webb, M.A.; Regier, T.Z.; Kokotin, V.; Beuneu, B.; Gemming, T.; et al. Atomic structure and formation of CuZrAl bulk metallic glasses and composites. *Acta Mater.* **2015**, *100*, 369–376. [CrossRef]
41. Callister, W.D. *Materials Science and Engineering: An Introduction*; John Wiley & Sons, Inc.: New York, NY, USA, 2007.